Quantum Paraelectric States in SrTiO3 and KTaO3: Barrett Model, Vendik Model, and Quantum Criticality

Quantum Paraelectric States in SrTiO₃ and KTaO₃: Barrett Model, Vendik Model, and Quantum Criticality

Hideshi Fujishita[1] [*], Shou Kitazawa[2], Masahiro Saito[2], Ryosuke Ishisaka[2], Hiroyuki Okamoto[3], and Toshihisa Yamaguchi[4]

[1] *School of Mathematics and Physics, Kanazawa University, Kanazawa 920-1192, Japan*

[2] *Division of Mathematical and Physical Sciences, Kanazawa University, Kanazawa 920-1192, Japan*

[3] *School of Health Sciences, Kanazawa University, Kanazawa 920-0942, Japan*

[4] *Department of Physics, School of Science and Engineering, Meisei University, Hino, Tokyo 191-8506, Japan*

The dielectric constants of the quantum paraelectrics SrTiO₃ and KTaO₃ are measured between 4 and 325 K. Their temperature dependences are analyzed on the basis of the Barrett and Vendik models. The former model deals with a ferroelectric optical mode coupled with other optical modes, whereas the latter deals with the mode coupled with acoustic modes. In addition, the latter contains a measure of the density of defects and inhomogeneity. The dielectric constants at low temperatures can be accurately described using Vendik's formula; however, they cannot be accurately described using Barrett's formula, even after the introduction of a measure of the density of defects and inhomogeneity. A critical quantum paraelectric region has been introduced recently between a classical region and a quantum paraelectric one. We point out that the critical region is where a low-temperature approximation is well realized for the model with the coupling between the ferroelectric and acoustic modes.

1. Introduction

Barrett extended Slater's classical theory of dielectric constants to BaTiO₃ more than 60 years ago by the quantum mechanical treatment of ionic polarizability.[1] This leads to a well-known expression, Barrett's formula, which is given as

$$\varepsilon(T) = \frac{C}{(T_1/2)coth(T_1/2T) - T_0} + \varepsilon_0, \tag{1}$$

---

[*]fujishit@staff.kanazawa-u.ac.jp

where C is the Curie constant, T_0 is the paraelectric Curie temperature, T is the sample temperature, and ε_0 is a temperature-independent constant, which was not included in the original formula. $T_1 = h\nu/k_B$, where k_B is the Boltzmann constant, h is the Planck constant, and $h\nu$ is the energy level difference of the harmonic part in the potential energy of the Ti ion. The system remains in a paraelectric state even at $T=0$ (a quantum paraelectric state) using this formula at $T_0 < T_1/2$. Later, this equation was derived lattice-dynamically on the basis of a model with a ferroelectric optical mode coupled with other optical modes, as mentioned in Ref. 2.

In 1979, Müller and Burkard measured the dielectric constant of monodomain $SrTiO_3$ along [110] between 0.3 and 300 K.[2] They analyzed the data on the basis of Eq. (1) without ε_0 as follows. The computed curve near 16 K diverged from the observed values and reached extremely low values at lower temperatures at T_1 of 80 K, where $C = 8.0 \times 10^4$ K and $T_0=35.5$ K. The temperature-independent dielectric constant at low temperatures was obtained by changing T_1 from 80 to 77.8 K, although the fit became poor between 4 and 70 K. This report has been widely considered a fundamental starting point for understanding quantum paraelectrics. For $KTaO_3$, Samara and Morosin measured the temperature dependence of the dielectric constant of $KTaO_3$ between 4 and 500 K in 1973.[3] They reported that the data fitted Eq. (1) very well over the entire temperature range. However, discrepancies were reported between several measurements and Eq. (1).

Various alternative models, in addition to the Barrett model, have been proposed to explain the quantum paraelectric state. In 1972, Vendik proposed a ferroelectric soft mode in $SrTiO_3$ represented as the motion of two sublattices coupled by a nonlinear elastic interaction.[4] He derived an equation to compute the square of the soft-mode frequency $\tilde{\omega}^2(T)$. This equation was later derived in a different but more general manner as[5]

$$\tilde{\omega}^2(T) = \omega_0^2 + \frac{9\hbar^2}{4k_B T_D} A \left[\frac{1}{2} + \frac{2}{(T_D/T)^2} \int_0^{T_D/T} \frac{x}{e^x - 1} dx \right], \tag{2}$$

where ω_0 is the frequency of the harmonic lattice vibration, A is the coupling constant in the fourth-order anharmonic term of the Hamiltonian, and $k_B T_D$ is the highest energy of the acoustic mode that couples with the harmonic lattice vibration. Equation (2) can be approximated as $\tilde{\omega}^2(T) \propto (T^2 - const.)$ for $T \ll T_D$ and $\tilde{\omega}^2(T) \propto (T - const.')$ for $T \gg T_D$. In 1997, Vendik and Zubko extended $\varepsilon(T)$ on the basis of Eq. (2), introducing the relation $\xi^2 = \xi_B^2 + \xi_S^2$, as[6]

$$\varepsilon(T) = \frac{C/T_0}{\left[\sqrt{\xi^2 + \eta^3} + \xi \right]^{2/3} + \left[\sqrt{\xi^2 + \eta^3} - \xi \right]^{2/3} - \eta} + \varepsilon_0, \tag{3}$$

where ξ_B is the normalized bias field, ξ_S is a measure of the density of defects and inhomogeneity, and

$$\eta = \frac{T_D}{2T_0}\left[\frac{1}{2} + \frac{2}{(T_D/T)^2}\int_0^{T_D/T}\frac{x}{e^x - 1}dx\right] - 1. \tag{4}$$

ε_0 in Eq. (3) was not included in the original formula. They analyzed the dielectric constant of $SrTiO_3$ below 180 K, whereas Zubko analyzed that of $KTaO_3$ below 80 K.[7]

Recently, the quantum fluctuations of electrical polarization have been proposed to produce a "rather unconventional" temperature dependence of the inverse dielectric constant at low temperatures, $1/\varepsilon \propto T^2$, in a quantum critical regime in the vicinity of a ferroelectric quantum critical point (QCP),[8,9] where an extended quantum critical theory was applied. The QCP is the point where a ferroelectric phase transition occurs by tuning a parameter at zero temperature. The parameter is either the hydrostatic pressure or an alternative chemical or isotropic substitution. A crossover between the quantum critical and quantum paraelectric regions was argued to exist, which decreased and disappeared at the QCP with a continuous change in the tuning parameter. The T^2 dependence of $1/\varepsilon$ was explained by the self-consistent phonon treatment of the soft ferroelectric optical mode.[8] The difference between the detailed temperature dependences of $1/\varepsilon$ at low temperatures for $SrTiO_3$ and $KTaO_3$ was explained by the difference between the values of their tuning parameters compared with the values at their QCPs.[8,10] Anharmonic interactions were taken into account between different wavevector modes of the transverse-optical branch in previous studies.[8,9] Then the behavior of the dielectric constant at very low temperatures follows Eq. (1). However, the quantum criticality theory was later revised to include the coupling of the electric polarization field with acoustic phonons.[10]

Several disagreements exist in the results of the analyses and interpretations based on these different models. A thorough examination of the digital data is necessary to investigate these models in detail. A structural phase transition at ~ 105 K in $SrTiO_3$ produces a multidomain distribution in a sample. The dielectic constants at low temperatures depend on the distribution which can be different from sample to sample because a monodomain crystal shows a large anisotropy of dielectic constants at low temperatures.[11] Thus, we performed careful measurements of the dielectric constants of $SrTiO_3$ and $KTaO_3$ between 4 and 325 K. We analyzed their temperature dependences on the basis of these models to determine the most appropriate model.

2. Experimental Details

The investigated sample of KTaO$_3$ was a top-seed-flux-grown crystal. A $10 \times 10 \times 0.5$ mm^3 plate with epi-polished (100) surfaces was supplied by MTI Corp. (USA). The investigated samples of SrTiO$_3$ were Verneuil-grown crystals. A $10 \times 10 \times 0.5$ mm^3 plate with mirror-polished (100) surfaces was supplied by Furuuchi Chemical Corp. (Japan). A plate with (110) surfaces was cut from a single-crystal boule obtained from Nakazumi Crystals Corp. (Japan). The (110) surfaces were finely polished using coated papers. These plates were cut to a size of $5 \times 5 \times 0.5$ mm^3. Electrodes with a typical area of 11.5 mm^2 were formed on the surfaces by gold evaporation. A (100) plate of SrTiO$_3$ with an electrode area of 2.0 mm^2 was also prepared to examine the effectiveness of corrections.

The dielectric constants ε' (real part) and ε'' (imaginary part) were measured using a precision LCR meter (HP 4284A) with an applied voltage of 500 mV. Measurements with an applied voltage of 5 mV were also performed to ensure a linear response to the applied electric field for the (100) plate of SrTiO$_3$. Measurements were performed for both heating and cooling processes. The temperature of the samples was controlled in the temperature range of 4–325 K using a helium closed-circuit refrigerator (Daikin Industries, CG308SBR).[12] An open/short/load correction method was adopted for the LCR meter, because preliminary measurements revealed that the normal open/short correction was insufficient for the high-dielectric-constant states of these materials, even in low-frequency measurements. A regularly used sample holder was also modified to ensure more precise measurements as follows. Two pairs of coaxial cables from the LCR meter used in a four-wire method were extended to the neighborhood of the sample. The longer distance between the sample and the end of the pair of coaxial cables was about 3 cm.

Least-squares fitting calculations of Barrett's formula were performed using the computer program KaleidaGraph. We also performed the least-squares fitting of Vendik's formula using the computer program Gnuplot, where a recursive-definition technique was employed for an integral function; no approximate expressions of the integral function were used.

3. Results

We did not observe any difference between the results obtained for the heating and cooling processes. In addition, no difference could be detected between the dielectric constants of SrTiO$_3$ along [100] obtained by applying voltages of 5 and 500 mV, which ensured a linear response to the applied electric field in the present measurements.

Figure 1 indicates the dielectric constant ε' (real part) of KTaO$_3$ along [100] as a func-
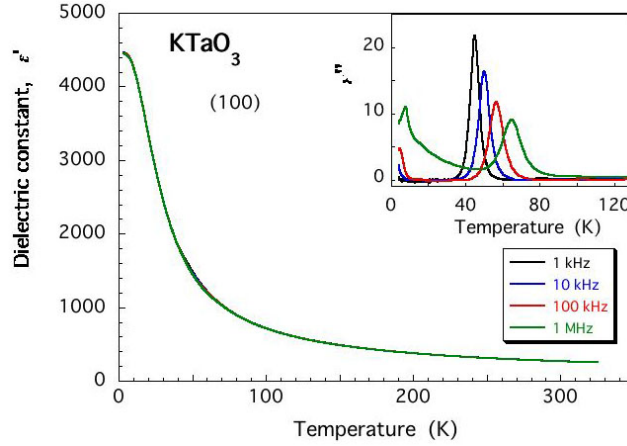
Fig. 1. (Color online) Dielectric constant ε' (real part) of KTaO$_3$ along [100] as a function of heating temperature. The inset shows the results for the dielectric constant ε'' (imaginary part). The dielectric constants were measured at frequencies of 1 kHz, 10 kHz, 100 kHz, and 1 MHz.

tion of heating temperature for frequencies of 1 kHz, 10 kHz, 100 kHz, and 1 MHz. The inset shows the dielectric constant ε'' (imaginary part). We could not detect any frequency dependences of the real parts. The imaginary parts were very small, but they showed peaks at different temperatures, that depended on the frequency. The temperature dependences of the real parts were essentially the same as those reported in Ref. 3, although the values for the real part were 15% smaller than our results.

The dielectric constant ε' (real part) of SrTiO$_3$ along [100] is delineated in Fig. 2 as a function of heating temperature for frequencies of 1 kHz, 10 kHz, 100 kHz, and 1 MHz. The inset shows the results for the dielectric constant ε'' (imaginary part). The electrode area of the specimen was 2.0 mm^2. The temperature dependences of the real parts for the specimen with an electrode area of 11.5 mm^2 were the same as those shown in Fig. 2, although the values were about 13% smaller than those shown in Fig. 2.

Figure 3 shows the dielectric constant ε' (real part) of SrTiO$_3$ along [110] as a function of heating temperature for frequencies of 1 kHz, 10 kHz, 100 kHz, and 1 MHz. The inset shows the results for the dielectric constant ε'' (imaginary part).

4. Analysis

An enhancement of the dielectric constant ε'' (imaginary part) below ~20 K was observed in KTaO$_3$ and SrTiO$_3$. Peaks were detected between ~45 and ~65 K, depending on the measured frequency, in ε'' for KTaO$_3$. We detected no clear dispersion of the dielectric constant ε' (real part). A feeble dispersion of ε' was found to exist at the temperatures of the peaks in

Fig. 2. (Color online) Dielectric constant ε' (real part) of SrTiO$_3$ along [100] as a function of heating temperature. The inset shows the results for the dielectric constant ε'' (imaginary part). The dielectric constants were measured at frequencies of 1 kHz, 10 kHz, 100 kHz, and 1 MHz.
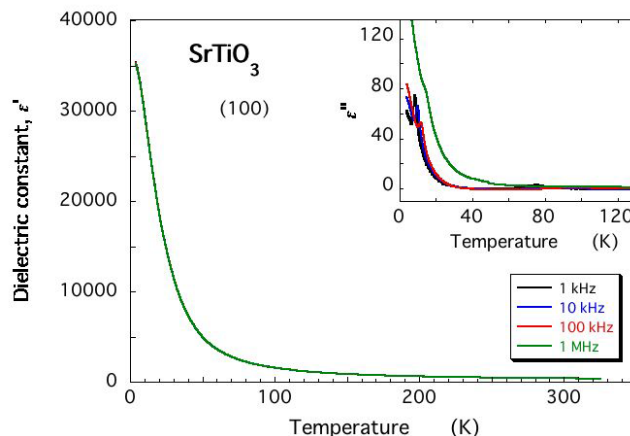

Fig. 3. (Color online) Dielectric constant ε' (real part) of SrTiO$_3$ along [110] as a function of heating temperature. The inset shows the results for the dielectric constant ε'' (imaginary part). The dielectric constants were measured at frequencies of 1 kHz, 10 kHz, 100 kHz, and 1 MHz.
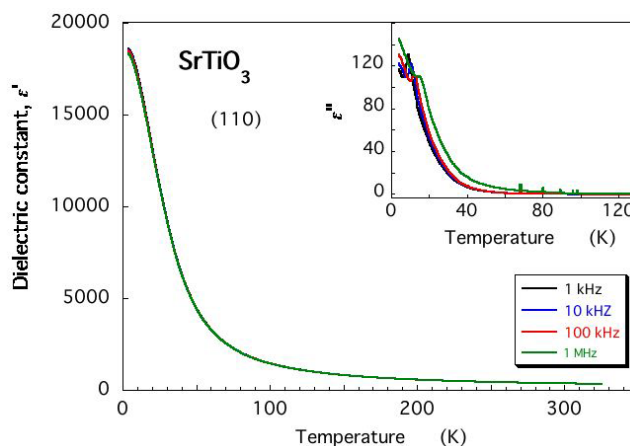
ε'' for KTaO$_3$. Extrinsic origins are considered to cause the enhancement and peak of ε'' as discussed in Sect. 5.1. Thus, we did not take them into account in the analyses of ε'.

4.1 *Analysis of* KTaO$_3$

Prior to the analyses using quantum mechanical formulae, the temperature dependence of the real part of the dielectric constant ε' of KTaO$_3$ along [100] measured at 10 kHz on heating above 150 K was analyzed using the classical Curie–Weiss formula, $\varepsilon = C/(T - T_0) + \varepsilon_0$. This analysis was conducted to determine whether the quantum mechanical formulae suffi-

ciently shifted to the classical one in this temperature range. The values are listed in Table I.

4.1.1 Analyses based on Barrett's formula

The temperature dependence of ε' for $KTaO_3$ measured at 10 kHz was analyzed on the basis of Barrett's formula, Eq. (1), between 4 and 325 K. The result is delineated in Fig. 4 by the red line (1) for the left axis. The green line (2) is a fit for T_1 and T_0 using the values given by Vogt[13] based on the analysis of hyper-Raman scattering data. The brown line (3) is a fit for T_1 and T_0 using the values given by Samara and Morosin.[3] The obtained values and corresponding values of χ^2 from these fittings are listed in Table I.

In the case of spectroscopic measurements, a least-squares fitting is usually performed on ω or ω^2, where the latter is proportional to $1/\varepsilon$ by the Lyddane–Sachs–Teller (LST) relation. In a constant-weight least-squares fitting, a larger value is considered to be more important than a smaller value. The quantum effects play an important role in the fitting of ε, while the classical effects play an important role in the fitting of $1/\varepsilon$. To see the difference, we conducted a fitting to A/ε', where the scale factor was set to 2554 $(cm^{-2}) \times 714.3$. The value of A was determined from the frequency in Ref. 13 and the dielectric constant obtained at 100 K. The fitting equation was $A/\varepsilon(T)$, where ε_0 was included in the denominator. The result of the fitting with no constraints on A/ε is delineated in Fig. 4 by the red line (1') for the right axis. The parameters and χ^2 values obtained by the fitting are listed in Table I.

4.1.2 Analyses based on Vendik's formula and comparison with those based on Barrett's formula

To compare the analyses based on Barrett's formula, Eq. (1), we first analyzed the data using Vendik's formula, Eq. (3), for $\xi = 0$, i.e.,

$$\varepsilon(T) = \frac{C/T_0}{\eta} + \varepsilon_0. \tag{5}$$

The lines in Fig. 5 indicate the results of least-squares fittings under various conditions. The red broken line shows the fit for $\xi = 0$, while the red solid line shows the fit for $\xi \neq 0$. The black solid line delineates the result of the fitting with fixed values of T_D and T_0 given by Zubko.[7] The parameters and χ^2 values obtained by these fittings are listed in Table I. The values obtained by the fitting of $A/\varepsilon(T)$ for $\xi \neq 0$ are listed in the table, although the fit is not delineated in Fig. 5 as it is impossible to distinguish the red line (1') in Fig. 4.

ξ is not included in Barrett's formula. The introduction of ξ greatly improved the fitting in Vendik's formula. To compare this result with the one obtained using Barrett's formula under
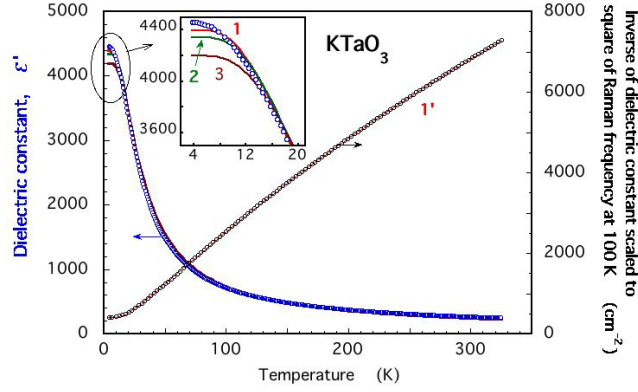
Fig. 4. (Color online) (Left) Results of fitting Barrett's formula to the dielectric constant ε' (real part) of KTaO$_3$ along [100], measured at 10 kHz on heating, where blue open circles are plotted at every 30 data points. The inset is an expansion of the low-temperature values of ε'. (Right) Results of fitting the inverse of Barrett's formula to A/ε', where the black open circles are plotted at every 100 data points, and $A = 2554$ (cm^{-2}) $\times$ 714.3. The red lines (1 and 1') are fits with no constraints. The green line (2) is a fit of T_1 and T_0 using Vogt's values.[13] The brown line (3) is a fit of T_1 and T_0 using Samara and Morosin's values.[3]

the same conditions, i.e., the introduction of ξ, η for Barrett's formula is given as

$$\eta = \frac{T_1}{2T_0} coth\left(\frac{T_1}{2T}\right) - 1. \tag{6}$$

The result of the fitting by Eqs. (3) and (6) is delineated by the blue solid line in Fig. 5. To discuss the quantum fluctuation effect later, the measured inverse dielectric constant and inverse of the red solid line are plotted against the square of the temperature up to approximately 32 K in the inset. The values obtained by this fitting and the χ^2 values are listed in Table I.

4.2 Analysis of SrTiO$_3$

Figure 6 shows a comparison between the values of the dielectric constant ε' (real part) of SrTiO$_3$ along different directions for different samples. The scales of the vertical axes were chosen to illustrate their maximum values. Maximum values of approximately 25,000 have been reported for the dielectric constants of monodomain crystals.[2,11] However, a value of about 43,000 based on dielectric measurement has been reported.[14] In addition, a value of about 40,000 has been estimated using hyper-Raman scattering measurements.[14,15] Our (100) plate sample with a maximum value of 36,000 was estimated to be a monodomain crystal, which required the introduction of a secondary order parameter, associated with the structural transition at 105 K, to analyze the dielectric constant.

In 1962, Sawaguchi et al. reported the results of dielectric measurements of SrTiO$_3$ along three directions, [100], [110], and [111], before the discovery of the structural transition. The
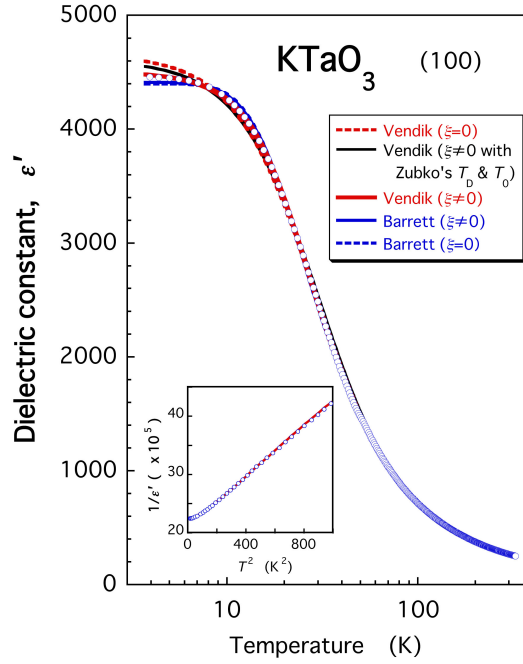
Fig. 5. (Color online) Comparison of fittings of Vendik's formula (red lines) and Barrett's formula (blue lines) to the dielectric constant ε' (real part) of KTaO$_3$ along [100], measured at 10 kHz on heating, where blue open circles are plotted at every 30 data points. The black line delineates the fit of T_D and T_0 using the values given by Zubko.[7] The broken and solid lines are fits for $\xi = 0$ and $\xi \neq 0$, respectively. The inset shows a comparison of the measured inverse dielectric constant and the inverse of the calculated value (the red solid line in the main figure) against the square of the temperature up to approximately 32 K.

dielectric constants differed very little from specimen to specimen.[16] Our result along [110] was almost the same as their result along [110]. Hehlen et al. reported hyper-Raman scattering data below 80 K,[17] combined with the previously reported data above 80 K by Vogt.[13] We obtained the frequencies in Fig. 1 from Ref. 17. The squares of the average frequency, $\tilde{\omega}^2$, below 80 K were obtained by taking their degeneracy into account, i.e., $\tilde{\omega}^2 = [\omega^2(A_{2u}) + 2\omega^2(E_u)]/3$. The average values are expected to be free from the effects of structural transition. The temperature dependence of $A/\tilde{\omega}^2$ is plotted using red open diamonds in Fig. 6, where A was taken to be 129.1 (cm^{-2}) $\times$ 18149 based on the dielectric constant and frequency at 6.9 K. Our dielectric constant data along [110] agrees well with $A/\tilde{\omega}^2$. Thus, our (110) plate sample was estimated to be almost an ideal random-domain crystal. Then, we analyzed the dielectric constant and inverse of the dielectric constant along [110], without taking the effect of the structural transition into account.

Prior to the analyses using quantum mechanical formulae, the temperature dependence of ε' measured at 10 kHz above 150 K was analyzed using the classical Curie–Weiss formula,

Table I. Comparison of values obtained for $KTaO_3$ by fitting Vendik's formula and Barrett's formula, as well as the Curie–Weiss formula ($T > 150$ K) under various conditions, where ξ is a measure of the density of defects and inhomogeneity. The scale factor A is equal to 2554 (cm^{-2}) × 714.3. The numbers in parentheses indicate the standard errors.

Formula	$C \times 10^4$ (K)	T_D or T_1 (K)	T_0 (K)	ε_0	ξ	$\chi^2 \times 10^5$
Curie–Weiss ($T > 150$ K)	6.282 (1)	—	4.54 (2)	54.27 (3)	—	—
Vendik ($\xi = 0$)	4.74 (2)	152.0 (5)	27.6 (2)	101.9 (6)	—	43.95
Vendik ($\xi \neq 0$)	5.769 (3)	86.5 (1)	13.16 (3)	66.7 (2)	0.667 (3)	1.52
Vendik ($\xi \neq 0$; fixed T_D & T_0 [1])	4.505 (2)	170	32.5	102.3 (4)	0.00 (9)	71.11
Barrett ($\xi = 0$)	6.032 (5)	51.39 (4)	11.80 (3)	55.2 (3)	—	15.13
Barrett ($\xi \neq 0$)	6.155 (9)	42.4 (4)	9.9 (1)	51.7 (4)	0.99 (3)	10.47
A/Vendik ($\xi \neq 0$)	6.064 (2)	64.5 (3)	9.72 (3)	60.88 (4)	1.262 (7)	5.34
A/Barrett ($\xi = 0$)	5.916 (2)	50.77 (6)	11.96 (4)	62.23 (4)	—	7.96

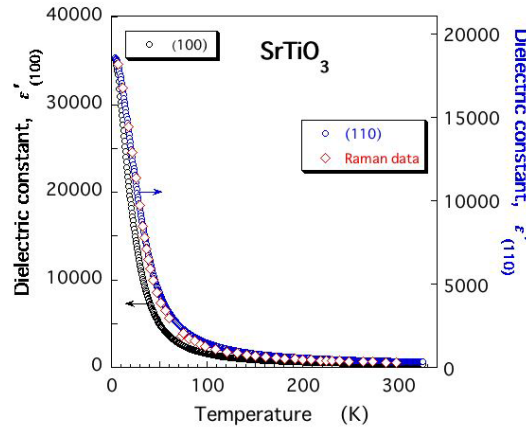[1]These values were fixed at the values obtained by Zubko.[7)]

Fig. 6. (Color online) Comparison of the dielectric constants ε' (real part) measured at 10 kHz on heating, and inverse of square of soft-mode frequency for $SrTiO_3$. The black open circles (left scale) and blue open circles (right scale) are dielectric constants along [100] and [110], respectively. The circles are plotted at every 20 data points. The red open diamonds are the squares of the inverse frequencies obtained by the hyper-Raman data,[13,17)] scaled to the dielectric constant at 6.9 K along [110]. The frequencies below 80 K are average values considering soft mode degeneracy.

$\varepsilon = C/(T - T_0) + \varepsilon_0$. The values are listed in Table II.

4.2.1 Analyses based on Barrett's formula

The blue and red lines in Fig. 7 show the results of the least-squares fittings of Eq. (1) to ε' for $SrTiO_3$ between 4 and 325 K for the left scale. The blue line delineates the result
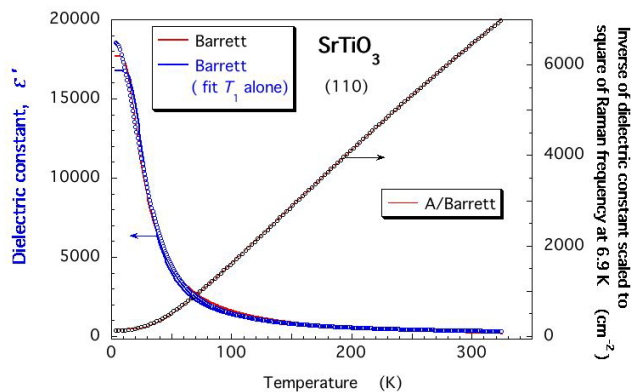
Fig. 7. (Color online) (Left) Results of fitting Barrett's formula to the dielectric constant ε' (real part) of SrTiO$_3$ along [110], measured at 10 kHz on heating, where blue open circles are plotted at every 30 data points. (Right) Results of the fitting of the inverse of Barrett's formula to A/ε', where the black open circles are plotted at every 100 data points, and A = 129.1 (cm^{-2}) $\times$ 18149. The red lines are fits with no constraints. The blue line is the result of the fit for T_1 alone, where C, T_0, and ε_0 are fixed at the values obtained by the fit of the Curie–Weiss formula above 150 K.

of the fitting using fixed values of C, T_0, and ε_0 obtained by fitting the Curie–Weiss formula above 150 K, while the red line indicates the result of fitting with no constraints. The result of the fitting to A/ε', without constraints for the right scale, is shown in Fig. 7. The fitting equation was $A/\varepsilon(T)$, where ε_0 was included in the denominator. The parameters and χ^2 values obtained by these fittings are listed in Table II.

4.2.2 Analyses based on Vendik's formula and comparison with those based on Barrett's formula

Analyses based on Vendik's formula were performed for the following three conditions: $\xi = 0$; $\xi \neq 0$; and $T_D = 175$ K, $T_0 = 42$ K, and $\xi \neq 0$, where the temperatures are those obtained for SrTiO$_3$ based on the same formula in Ref. 6. The results of the fittings are shown by a red broken line, red solid line, and black solid line, respectively, in Fig. 8. The fitting of Barrett's formula with $\xi \neq 0$ [using Eqs. (3) and (6)] was also conducted for comparison. The result is drawn using a blue solid line in Fig. 8, where the result for $\xi = 0$ is shown by a blue broken line again. A comparison of the measured inverse dielectric constants along [110] and [100] and the inverse of the red solid line (i.e., fit to ε' along [110]) is plotted against the square of the temperature up to 50 K in the inset. The values and χ^2 values obtained by these fittings are listed in Table II.
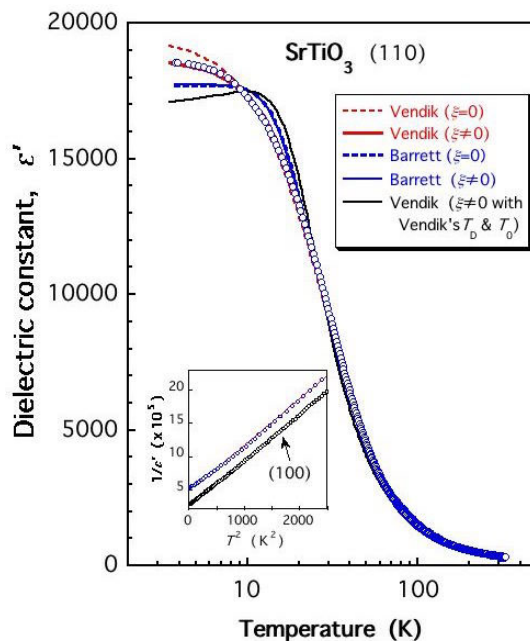
Fig. 8. (Color online) Comparison of fittings of Vendik's formula (red lines and black line) and Barrett's formula (blue lines) to the dielectric constant ε' (real part) of SrTiO$_3$ along [110], measured at 10 kHz on heating, where blue open circles are plotted at every 20 data points. The broken and solid lines are fits for $\xi = 0$ and $\xi \neq 0$, respectively. The inset shows a comparison of the measured inverse dielectric constants along [110] (blue open circles) and [100] (black open circles) and the inverse of the calculated value (red solid line, which is the inverse of the red solid line in the main figure) against the square of the temperature up to approximately 50 K.

5. Discussion

5.1 Enhancements and peaks in dielectric constant ε'' (imaginary part)

Enhancements of the dielectric constant ε'' (imaginary part) were observed below ~20 K for KTaO$_3$ and SrTiO$_3$. Peaks in the dielectric constant ε' (real part) at 10–20 K and the ferroelectric properties below these temperatures were frequently observed in the early stages of the studies for both materials.[18, 19] These ferroelectric phases were attributed to extrinsic origins such as the impurities and conditions of the sample preparation[18] or oxygen vacancies.[20] Recent crystals do not show such peaks. However, factors with extrinsic origins affecting the damping of the ferroelectric soft modes at low temperatures might exist even in recent crystals, causing the enhancement of ε'' below ~20 K in the present measurements.

Very small peaks in the dielectric constant ε'' were detected between ~45 and ~65 K, which depended on the measured frequency, for KTaO$_3$ in addition to the enhancement. A slight modulation of the temperature dependence of ε' was observed around the corresponding temperature, which cannot be described by Eq. (3). An anomaly in the exponent γ

Table II. Comparison of values obtained for $SrTiO_3$ by fitting Vendik's formula and Barrett's formula, as well as the Curie–Weiss formula ($T > 150$ K), under various conditions, where ξ is a measure of the density of defects and inhomogeneity. The scale factor A is 129.1 (cm^{-2}) $\times$ 18149. The numbers in parentheses indicate the standard errors.

Formula	$C \times 10^4$ (K)	T_D or T_1 (K)	T_0 (K)	ε_0	ξ	χ^2
Curie–Weiss ($T > 150$ K)	8.022 (2)	—	45.65 (2)	47.06 (6)	—	—
Vendik ($\xi = 0$)	9.19 (1)	273 (4)	64.1 (9)	-100 (5)	—	2.280 $\times 10^8$
Vendik ($\xi \neq 0$)	7.91 (5)	281 (2)	67.1 (5)	5 (2)	0.0098 (3)	2.676 $\times 10^7$
Vendik ($\xi \neq 0$; fixed T_D & T_0 [2])	9.20 (2)	175	42	71 (4)	0.0315 (1)	1.253 $\times 10^9$
Barrett ($\xi = 0$)	15.53 (6)	66.2 (2)	24.5 (2)	-325 (4)	—	4.917 $\times 10^8$
Barrett ($\xi \neq 0$)	15.8 (2)	64 (2)	23.5 (6)	-335 (6)	0.08 (3)	4.888 $\times 10^8$
A/Vendik ($\xi \neq 0$)	6.992 (3)	298.9 (1)	72.32 (3)	65.33 (4)	0.00867 (3)	7.307 $\times 10^4$
A/Barrett ($\xi = 0$)	7.755 (4)	125.9 (2)	57.21 (6)	48.6 (2)	—	2.371 $\times 10^6$

[2] These values were fixed at the values obtained by Vendik and Zubko.[6]

obtained by a power law fit ($\delta\varepsilon'^{-1} \sim T^\gamma$) was observed at 40 K in $KTaO_3$,[8] which was considered to be an extrinsic effect related to oxygen vacancies, where $\delta\varepsilon'^{-1}$ denotes the change in the inverse dielectric constant ε' from its zero temperature value. Detailed studies on the anomaly of ε'' for $KTaO_3$ are desirable because they seem lacking compared with the studies in $SrTiO_3$.[20]

5.2 Quantum paraelectric state in $KTaO_3$

The present temperature dependence of the real part of the dielectric constant ε' of $KTaO_3$ was essentially the same as the dependence reported by Samara and Morosin,[3] with only a 15% difference in the values. However, the results of the analyses based on Eq. (1) are very different. Our fit shows saturation and deviates from the observations below 8 K as delineated by the red line (1) in Fig. 4, in contrast to the very good fit between 4 and 500 K of their analysis (Fig. 2 of Ref. 3). In addition, when using their values of T_1 and T_0, our fit deviates from the observations below 15 K and saturates below 8 K, as shown by the brown line (3) in Fig. 4. Although their values of T_1 and T_0 are 11% greater than ours, their values of C and ε_0 agree very well with our values if the 15% difference between the observed dielectric constants is taken into account. The values are compared in Table III. To clarify the cause of the discrepancy, we calculated the dielectric constants on the basis of their values and compared them with their observations. This calculation shows the deviation from their observations below 15 K, in contrast to their calculation.

Vogt measured a soft-mode frequency of $KTaO_3$ using hyper-Raman scattering,[13] which agreed well with the dielectric constant previously measured[3] using the LST relation. He analyzed the frequency using Barrett's formula, combined with a high-temperature limit of the soft-mode frequency, i.e., an analysis using $[A/Eq.(1)]^{1/2}$. He reported an accurate reproduction of the data by this analysis. However, the dielectric constant at low temperatures cannot be reproduced by Eq. (1) with the values in Ref. 3. We calculated the frequency using the values represented in Ref. 13 and found that there were slight differences between the calculated and observed frequencies at low temperatures.

Because $(2T/T_1)/coth(T_1/2T) > 0.99$ for $T_1 = 51.4$ K and $T > 150$ K, Eq. (1) is expected to sufficiently shift to the Curie–Weiss formula. However, the values of T_0 in Table III are at least 2.6 times greater than the value presently obtained by applying the Curie–Weiss formula for $T > 150$ K. This indicates that Eq. (1) is insufficient to describe the dielectric constant of the quantum paraelectric state of $KTaO_3$, in addition to its inability to describe the dielectric constant at low temperatures.

Vendik's formula, Eq. (3), can be fitted well to ε' for $KTaO_3$ at all the measured temperatures. The formula contains ξ, a measure of the density of defects and inhomogeneity. The introduction of ξ to Barrett's formula only slightly improved the fitting of ε', whose χ^2 is seven times greater than that of the fit by Eq. (3). Thus, it can be concluded that Vendik's formula is more appropriate for describing the dielectric constant of the quantum paraelectric state in $KTaO_3$ than Barrett's formula. The result of the fitting of Eq. (3) by Zubko[7] was very different from our result. The values of T_D and T_0 were 2 and 2.5 times greater than our values, respectively. There might be two reasons for these differences. (1) The data used were limited below 80 K and (2) ε_0 was excluded from the equation they fitted.

The values of T_D and T_0 obtained by fitting $A/[Eq. (3)]$ to A/ε' are 25% smaller than the values obtained by fitting Eq. (3) to ε', as listed in Table I. Thus, we should be careful in comparing the results obtained by different methods. In addition, we should note that the effect of ξ on the soft-mode frequency obtained by scattering experiments might be different from that on the dielectric constant, because the former is a microscopic property, while the latter is a macroscopic property.

5.3 *Quantum paraelectric state in* $SrTiO_3$

Vogt suggested the occurrence of a ferroelectric phase transition in the absence of structural distortion in $SrTiO_3$.[13] He analyzed the hyper-Raman scattering data, including the weighted-average frequency below the structural transition temperature, where the degener-

Table III. Comparison of present values with those previously reported for $KTaO_3$ by fitting Barrett's formula, as well as those of the Curie–Weiss formula ($T > 150$ K). The numbers in parentheses indicate the standard errors.

Formula	$C \times 10^4$ (K)	T_1 (K)	T_0 (K)	ε_0
Curie–Weiss ($T > 150$ K)	6.282 (1)	—	4.54 (2)	54.27 (3)
Barrett (present)	6.032 (5)	51.39 (4)	11.80 (3)	55.2 (3)
Barrett (previous) [3]	5.45	56.9	13.1	47.5
A/Barrett (present)	5.916 (2)	50.77 (6)	11.96 (4)	62.23 (4)
$[A$/Barrett$]^{1/2}$ (previous) [4]	—	55	14	—

[3]These values were fixed at the values obtained by Samara and Morosin.[3] [4]These values were fixed at the values obtained by Vogt.[13]

acy of the ferroelectric A_{2u} and E_u modes was considered while computing their weights. The analysis was made using Barrett's formula, Eq. (1), including the temperature dependence of T_1 associated with the structural distortion. The result indicated that a ferroelectric phase transition occurred at around 35 K if there was no structural distortion. However, the average frequency based on the degeneracy is expected to be independent of the effect of structural distortion, because the frequency exhibits a cubic symmetry. Thus, it is unnecessary to introduce an order parameter associated with the structural distortion to the analysis of the average frequency.

On the basis of an analysis of the results of precise hyper-Raman scattering experiments, Yamanaka et al. concluded that the quantum paraelectric state of $SrTiO_3$ was stabilized by the structural distortion, and if there was no distortion, $SrTiO_3$ would undergo a ferroelectric phase transition at around 30 K.[15] However, in this analysis, the frequencies of both the A_{2u} and E_u modes were higher than the frequency of the ferroelectric mode in the absence of the structural distortion. This means that the A_{2u} and E_u modes do not couple with the structural transition. In other words, this was an anti-coupling solution of the equation they solved, which has two solutions.

A random domain structure is a good approximation for the presently measured (110) plate sample for the reason stated in Sect. 4.2. The temperature dependence of the real part of the dielectric constant ε' of $SrTiO_3$ at low temperatures can be fitted well using Vendik's formula, whereas it cannot be fitted using Barrett's formula, even if ξ is introduced to the formula. The difference in the fittings is clear in Fig. 8. The fitting of Vendik's formula, using the temperatures T_D and T_0 from Refs. 6 and 21, shows a deviation below 20 K and a peak at 10 K. The temperature of the peak can be confirmed using the condition $\partial \varepsilon / \partial T = 0$ for

Eq. (3), i.e., T for $\xi^2 = \eta^3$.[6] Thus, the fitting, delineated by the black solid line in Fig. 8, was accurately performed. The maximum values of the dielectric constants in Refs. 6 and 21 are $\sim$25,000, which are almost the same as those in monodomain crystals.[2,11] Thus, a random-domain approximation is inadequate for the data in Refs. 6 and 21, and it is necessary to introduce the effects of structural distortion in the analyses.

The values of T_D and T_0 obtained by the fitting of $A/$[Eq. (3)] to A/ε' are about 7% greater than the values obtained by fitting Eq. (3) to ε'. Thus, we should be careful when we compare the results obtained by different methods. In addition, we should note that the effect of ξ on the soft-mode frequency obtained by scattering experiments might be different from that on the dielectric constant, even though the value is very small compared with that for KTaO$_3$.

5.4 Comparison with analyses based on quantum critical theory

The nonclassical T^2 dependences of the inverse dielectric constant ε' (real part) observed in both crystals have been understood in terms of the quantum critical theory extended to include the effects of long-range dipolar interactions as follows:[10] The relation $\varepsilon_0 \boldsymbol{E} = a\boldsymbol{P} + b\boldsymbol{P}^3 - c\nabla^2 \boldsymbol{P}$ between the polarization $\boldsymbol{P}$ and the electric field $\boldsymbol{E}$ is assumed at absolute zero, where ε_0 is the dielectric constant of vacuum, a is the inverse static susceptibility, b is the mode-mode coupling parameter, and c is the mode stiffness parameter. By setting a equal to zero, the inverse electric susceptibility at finite T, $1/\chi(T)$, satisfies the self-consistent equation

$$1/\chi(T) = g_2 bc^2 k_B T \int_0^{q_T} \frac{q^{d-1}dq}{cq^2 + 1/\chi(T)}, \tag{7}$$

where g_2 is a numerical constant, q_T is a thermal cutoff wavevector, and d denotes the dimension of the system. The temperature dependence of the dielectric constant was obtained by numerically solving Eq. (7) without using adjustable parameters. By introducing a dynamical exponent z defined as $\omega_q \propto q^z$, one can find that $1/\chi(T) \propto T^{(d+z-2)/z}$. For displacive ferroelectrics with $d = 3$ and $z = 1$ near the QCP, $1/\chi(T)$ can be approximately expressed as

$$1/\chi(T) = a + \frac{5\varepsilon_0 k_B^2 b}{18\hbar cv} T^2, \tag{8}$$

where v is the velocity of the coupled mode, $\hbar\Delta$ is the energy gap of the mode at $q = 0$, and $c = av^2/\Delta^2$. The temperature dependence of Eq. (8) is expected to cross over to an exponential form in the quantum paraelectric region if the transverse optical mode does not condense.

We can easily presume the form of Eq. (8) except the expression for the modulus of T^2. This is because the equation is essentially the same as the low-temperature approximation of Eq. (2); however, their derivations are different. The modulus is expressed using universal

constants and quantities that can be determined by independent measurements. We can verify the validity of Eq. (8) by comparing the values with the experimental values, in addition to the correctness of numerical solutions of Eq. (7) without adjustable parameters.[10]

The values obtained for KTaO$_3$ and SrTiO$_3$ from Ref. 10 are listed in Table IV. The low-temperature limit T^* of the T^2 dependence of $1/\varepsilon'$ for KTaO$_3$ and the gradients for KTaO$_3$ and SrTiO$_3$ were obtained from Figs. 2 and 3 in Ref. 10. The gradients in the last column of the table were obtained from Eq. (8) using the specific parameters provided in Table I of Supplementary Information in Ref. 10. The values obtained by the present measurements and analyses for KTaO$_3$ and SrTiO$_3$ are also listed in the table. We analyzed the observed data by fitting Eqs. (3) and (4). Then, the calculated gradients were in good agreement with the observed ones.

T^* and the observed gradient for KTaO$_3$ were similar in both measurements. The calculated gradients in Ref. 10 were 1/3.6 and 1/1.8 times those of the observed values in Ref. 10 . Thus, the calculated gradients in Ref. 10 were not in good agreement and also different from the observed value.

The observed gradients for SrTiO$_3$ in both measurements were similar; however, the T^* value was different. Although the deviation from the T^2 dependence of $1/\varepsilon'$ was not observed above 2 K in Ref. 10, T^* was approximately 22 K in the present measurement. As stated in Sect. 4.2, the (110) sample can be considered as a nearly ideal random-domain crystal. Considering the low-temperature value of ε' in the (100) sample, this crystal can be considered as a nearly monodomain crystal, whose T^2 dependence of $1/\varepsilon'$ was observed above 4 K, as shown in the inset of Fig. 8. Then, the crystals measured in Ref. 10 might slightly deviate from the ideal random-domain structure. The calculated gradients in Ref. 10 were 1/2 and 1.3 times those of the observed values in Ref. 10. Thus, the calculated gradients in Ref. 10 were not in good agreement and also different from the observed values.

A quantum tuning parameter $g = a/c\Lambda^2$, which can be varied either by pressure or alternatively by chemical or isotopic substitution, vanishes at QCP, where Λ is the effective Debye wavevector.[10] Using the values provided in Table I of Supplementary Information in Ref. 10, we obtain $g_{KTO}/g_{STO} = 0.010/0.0023 \approx 4.3$, although a factor of 2π appears to be lacking in the expression for Λ, where g_{KTO} and g_{STO} are the tuning parameters for KTaO$_3$ and SrTiO$_3$, respectively. The temperature normalized to the effective Debye temperature $\theta = \hbar v\Lambda/k_B$ is plotted against g in the phase diagram for a displacive ferroelectric in Fig. 4 in Ref. 10. The relationship of $(T^*/\theta)_{KTO} \gg (T^*/\theta)_{STO}$ is expected on the basis of this diagram. However, a ratio of $(T^*/\theta)_{KTO} = 0.78(T^*/\theta)_{STO}$ was obtained in the result of this study, which does not

agree with the phase diagram, although the basis of the tuning parameter dependence of T^*/θ is not shown.

Finally, the critical quantum paraelectric region introduced in Ref. 10 is where a low-temperature approximation is well realized for the model with the coupling between the ferroelectric and acoustic modes. The analyses without the adjustable parameters did not successfully describe the measurements quantitatively.

Table IV. Comparison of values of the low-temperature limit T^* of the T^2 dependence of $1/\varepsilon'$ for KTaO$_3$ and SrTiO$_3$. The gradients of the T^2 dependence above T^* are also compared.

Specimen	T^*(obs) (K)	Gradient (obs) ($\times 10^{-8}K^{-2}$)	Gradient (cal) ($\times 10^{-8}K^{-2}$)	Gradient (cal) ($\times 10^{-8}K^{-2}$)
KTaO$_3$ (Ref. 10)	~12 [5]	25 [5]	6.9 [5]	14 [6]
KTaO$_3$ [present (100)]	~12	21	22	-
SrTiO$_3$ (Ref. 10)	$\leq$ 2 [7]	8.2 [5]	4.2 [5]	11 [6]
SrTiO$_3$ [present (110)] [8]	~22	7.1	7.0	-
SrTiO$_3$ [present (100)] [9]	$\leq$ 4 [7]	6.9	-	-

[5]These values were obtained from figures in Ref. 10. [6]These values were calculated on the basis of Eq. (8). [7]T^* was not detected above this temperature. [8]This sample can be considered as a nearly ideal random-domain crystal. [9]This sample can be considered as a nearly monodomain crystal.

6. Conclusions

The dielectric constants of the quantum paraelectric states of SrTiO$_3$ and KTaO$_3$ at low temperatures can be well described using Vendik's formula, which is based on the coupling between the ferroelectric and acoustic modes. It also includes a measure of the density of defects and inhomogeneity. The dielectric constants at low temperatures cannot be described properly using Barrett's formula, even after the introduction of a measure of the density of defects and inhomogeneity. The critical quantum paraelectric region recently introduced in Ref. 10 is where a low-temperature approximation is well realized for the model with the coupling between the ferroelectric and acoustic modes.

References

1) J. H. Barrett, Phys. Rev. **86**, 118 (1952).

2) K. A. Müller and H. Burkard, Phys. Rev. B **19**, 3593 (1979).

3) G. A. Samara and B. Morosin, Phys. Rev. B **8**, 1256 (1973).

4) O. G. Vendik, Sov. Phys. Solid State **14**, 849 (1972).

5) S. Nishi, H. Kawamura, and K. Murase, Phys. Status Solidi **97**, 581 (1980).

6) O. G. Vendik and S. P. Zubko, J. Appl. Phys. **82**, 4475 (1997).

7) S. P. Zubko, Tech. Phys. Lett. **24**, 839 (1998).

8) S. E. Rowley, L. J. Spalek, R. P. Smith, M. P. M. Dean, G. G. Lonzarich, J. F. Scott, and S. S. Saxena, arXiv: 0903.1445.

9) R. Blinc, *Advanced Ferroelectricity* (Oxford University Press, Oxford, 2011) p. 12.

10) S. E. Rowley, L. J. Spalek, R. P. Smith, M. P. M. Dean, M. Itoh, J. F. Scott, G. G. Lonzarich, and S. S. Saxena, Nat. Phys. **10**, 367 (2014).

11) T. Sakudo and H. Unoki, Phys. Rev. Lett. **26**, 851 (1971).

12) T. Yamaguchi and S. Sawada, J. Phys. Soc. Jpn. **60**, 3162 (1991).

13) H. Vogt, Phys. Rev. B **51**, 8046 (1995).

14) H. Uwe and T. Sakudo, Phys. Rev. B **13**, 271 (1976).

15) A. Yamanaka, M. Kataoka, Y. Inaba, K. Inoue, B. Hehlen, and E. Courtens, Europhys. Lett. **50**, 688 (2000).

16) E. Sawaguchi, A. Kikuchi, and Y. Kodera, J. Phys. Soc. Jpn. **17**, 1666 (1962).

17) B. Hehlen, L. Arzel, A. K. Tagantsev, E. Courtens, Y. Inaba, A. Yamanaka, and K. Inoue, Physica B **263-264**, 627 (1999).

18) F. Jona and G. Shirane, *Ferroelectric Crystals* (Dover Publications, Inc., New York, 1993) p. 225; ibid, p. 250.

19) D. G. Demurov and Yu. N. Venevitsev, Fiz. Tverd. Tela **13**, 669 (1971) [Sov. Phys. - Solid State **13**, 553 (1971)].

20) J. F. Scott, J. Phys.: Condens. Matter **11**, 8149 (1999).

21) R. G. Geyer, B. Riddle, J. Krupka, and L. A. Boatner, J. Appl. Phys. **97**, 104111 (2005).